이학석사학위논문

Supramolecular Nanofibers as Multivalent Ligands of Regulating Bacterial Cell Agglutination

다중 리간드 역할을 하는 초분자 나노섬유의 박테리아 응집 조절

2013년 2월

서울대학교 대학원

화학부 유기화학 전공

김 태 훈

Supramolecular Nanofibers as Multivalent Ligands of Regulating Bacterial Cell Agglutination

다중 리간드 역할을 하는 초분자 나노섬유의 박테리아 응집 조절

지도교수 박 충 모

이 논문을 이학석사학위논문으로 제출함

2012년 12월

서울대학교 대학원

화학부 유기화학 전공

김 태 훈

김태훈의 석사학위논문을 인준함

2012년 12월

위 원 장 최태림 (인)

부 위 원 장 박충모 (인)

위 원 이 연 (인)

Abstract

Supramolecular Nanofibers as Multivalent Ligands of Regulating Bacterial Cell Agglutination

Taehoon Kim
Department of Chemistry
The Graduate School
Seoul National University

Control of the size and shape of molecular assemblies on the nanometer scale in aqueous solutions is very important for the regulation of biological functions. Among the well-defined supramolecular structures of organic amphiphiles, one-dimensional nanofibers have attracted much attention because of their potential applications in biocompatible materials. Although much progress has been made in the field of self-assembled nanofibers, the ability to control the fiber length remains limited. The approach for control of the fiber length presented herein overcomes this limitation through the coassembly of amphiphilic rod−coil molecules in which the crystallinity of the aromatic segment can be regulated by π−π stacking interactions. The introduction of carbohydrate segments into the fiber exterior endows the nanofibers with the ability to adhere to bacterial cells. Notably, the fiber length systematically regulates the agglutination and proliferation of bacterial cells exposed to these fibers.

keywords : multivalent ligands, carbohydrate-coated nanofiber, self-assembly length control, agglutination, proliferation of bacterial cells

***Student Number* : 2010-20272**

Contents

Supramolecular Nanofibers as Multivalent Ligands of Regulating Batecrial Cell Agglutination

LIST OF TABLES

LIST OF SCHEMES

LIST OF FIGURES

Supramolecular Nanofibers as Multivalent Ligands of Regulating Bacterial Cell Agglutination

1. Introduction

One of the fascinating features of carbohydrate-coated nanofibers is their multivalent interactions with specific biomolecules. A recent series of studies revealed that the carbohydrate-coated one-dimensional nanostructures formed through the self-assembly of small carbohydrate-containing molecules, such as discotic compounds[1] and peptide amphiphiles.[2−6] specifically bind to multiple mannose-binding proteins. These fibrillar structures coated by carbohydrates are excellent multivalent ligands for specific receptors on cell surfaces[7, 8] and can modulate carbohydrate−receptor binding events associated with biological processes.[9, 10] Although much progress has been made in the field of carbohydrate nanofibers, the ability to control the length of carbohydrate-coated nanofibers remains limited. To date, only a few methods have been reported to control fiber length in self-assembled systems, irrespective of the biological functions of these systems. The research group of Manners and Winnik reported that the length of mono disperse cylindrical micelles could be well-controlled in organic solvent by crystallization-driven living self-assembly of block copolymers.[11−13] Besenius et al. reported another approach, charge repulsion, to control the length of nanofibers in water.[14] Another example is the template approach, in which dumbbell-shaped rod amphiphiles are used as templates for peptide assembly on their surfaces to form nanofibers with a controlled length.[15] Lee et al. previously reported that a

rigid−flexible combination in an amphiphilic system leads to the formation of nanofibers with a well-defined width in aqueous solutions. These nanofibers are based on an amorphous aromatic core that undergoes a sol−gel interconversion in response to external stimuli.[16−18] I hypothesized that varying the crystallinity of the aromatic cores in nanofibers would regulate the fiber length by controlling the π-π stacking interactions. With this idea in mind, I performed coassembly experiments to regulate the crystallinity of the aromatic cores of carbohydrate nanofibers for the purpose of controlling the fiber length, which might in turn control the biological functions of bacterial cells by altering the multivalent interactions.

2. Results and Discussion

In this communication, I report the ability to control the length of carbohydrate-coated nanofibers through the coassembly of carbohydrate rod amphiphile **1**, which has a highly crystalline aromatic core, with **2**, which has a less crystalline aromatic core than **1** (Figure 1). With increasing content of **2**, the fiber length decreases

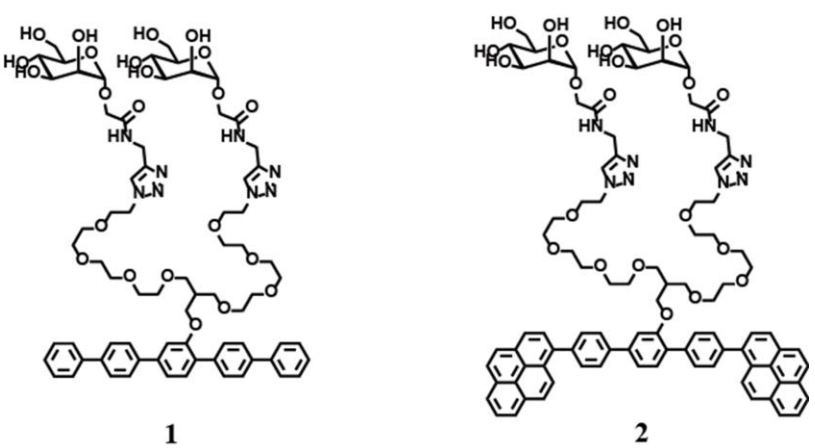

Figure 1. Chemical structures of amphiphiles **1** and **2**.

from a few micrometers to a few tens of nanometers as the result of the decreasing crystallinity of the aromatic cores. These nanofibers bind bacterial cells through multivalent carbohydrate-receptor interactions and systematically regulate the proliferation of the bacterial cells, with the effect depending on the fiber length. The amphiphiles that form these nanofibers consist of aromatic segments that are laterally grafted by hydrophilic mannose moieties. These amphiphilic molecules were synthesized in a stepwise fashion according to the procedure described in the experimental section. The resulting aromatic amphiphiles were characterized by NMR spectroscopy and MALDI−TOF mass spectrometry, and the results were in full agreement with the structures presented herein (Figure 7-9 in experimental section).

The formation of self-assembled nanostructures was initially investigated by transmission electron microscopy (TEM). In addition, cryogenic TEM (cryo-TEM) was also undertaken to investigate the self-assembled structures in bulk solutions. Figure 2 shows micrographs obtained for 60 μM aqueous solutions of **1**, **2**, and coassembled amphiphiles cast onto TEM grids. The TEM image of **1**, which is based on pyrene units and was negatively stained with uranyl acetate, clearly shows long, rigid nanofibers with a uniform width of ~6 nm and lengths of > 2 μm. I could not accurately measure the lengths of the nanofibers because the fibers extended beyond the boundary of the TEM image. In contrast, **2**, which is based on a pentaphenylene rod, self-assembles into short fibers with an average length of 70 nm. The combination of these two nanofibers through coassembly might result in the formation of nanofibers with different lengths. To test this hypothesis, I performed coassembly experiments with **1** and **2**. Interestingly, the length of the nanofibers systematically decreased from a few micrometers to less than 70 nm as

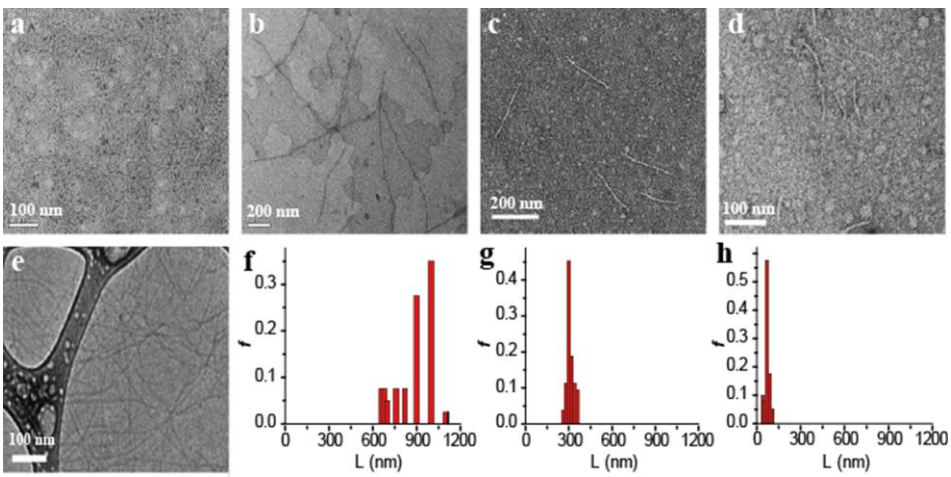

Figure 2. TEM images of (a) **1** (60 μM) in water and (b−d) coassembled samples with decreasing nanofiber length and increasing proportion of **2**: (b) **1**:**2** = 85:15; (c) **1**:**2** = 50:50; (d) **2**. (e) Cryo-TEM image of **1**. (f−h) Contour length distributions (f) of samples (b−d), respectively.

the amount of **2** increased. When the length distribution of the nanofibers based on measurements of >150 fibers in the images was evaluated, the average lengths of the nanofibers were 1 μm, 300 nm, and 70 nm for **1**:**2** mole ratios of 85:15, 50:50, and 0:100, respectively.

To gain insight into the packing arrangements of the rod segments in nanofibers of different lengths, I used UV−VIS absorption and fluorescence emission spectroscopy (Figure 3a). When the coassembled samples were excited at the wavelength of absorption maximum of **2**, the wavelength of emission maximum of **2** was gradually red-shifted and quenched with increasing **1** content, which suggested that the energy transfer process between two amphiphiles occurred more efficiently, indicating that there are increasing π-π stacking interactions. To assess further the packing arrangements of the aromatic cores of **1**, **2**, and the coassembled

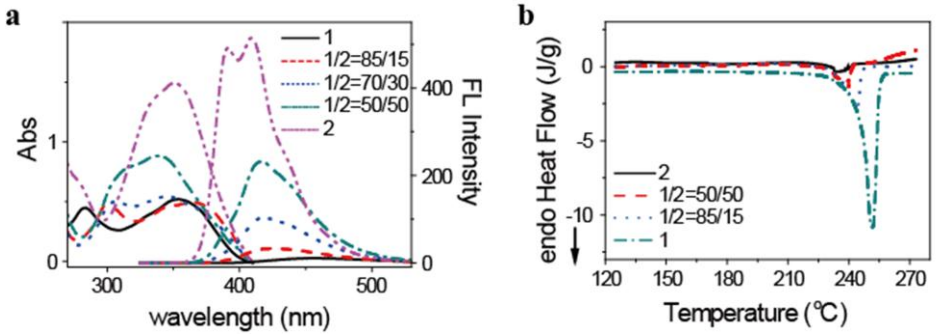

Figure 3. (a) UV/VIS absorption and Fluorescence emission spectra of amphiphiles **1** and **2** (60 μM) in water upon excitation at 316 nm. (b) DSC traces for **1**, **2**, and coassembled amphiphiles upon heating.

amphiphiles, the thermal behavior of the freeze-dried samples was evaluated by differential scanning calorimetry (DSC). The melting transition temperatures (T_m) and the corresponding enthalpy changes of all of the samples obtained from the DSC heating scans (Figure 3b) are summarized in Table 1. As shown in Figure 3b and Table 1, an increase in the relative amount of **2** led to a shift in the melting point to lower temperatures along with a significant decrease in the heat of fusion, demonstrating that the crystallinity of the aromatic core of **1** is disrupted by the addition of **2**. These results suggest that the packing arrangements within the aromatic core play a critical role in controlling the length of the self-assembled

Sample	T_m of heating (^oC)	Enthalpy of fusion (J/g)	Relative crystallinity[a] (%)
only **1**	251	131	100
1:**2**=85:15	243	90	69
1:**2**=50:50	239	43	33
only **2**	233	27	21

[a]Relative Crystallinity (%) = {ΔH_f (sample) / ΔH_f (**1**)} x 100

Table 1. Thermal behavior of **1**, **2** and co-assembled amphiphiles.

nanofibers. Indeed, the high crystallinity of the aromatic core of **1**, as reflected by the large heat of fusion, leads to the formation of long nanofibers with a micrometer-scale length. In contrast, amorphous aromatic cores with very low heats of fusion, as in the case of **2**, give rise to short fibers with lengths of only a few tens of nanometers. The systematic replacement of pyrene units with phenyl units through coassembly would result in the disruption of the packing of the aromatic segments, thereby reducing the assembly forces of the molecules. Consequently, the fiber length of **1** systematically decreased with the successive addition of **2**.

To gain further insight into the variation in the length of the fibers, I measured the solution viscosity and performed static light scattering (SLS) experiments. The solution viscosities of **1**, **2**, and the coassembled amphiphiles were measured at 27℃ using a capillary viscometer. The results showed that the viscosity dramatically increases with an increase in the relative amount of **1** (Figure 4a). This result could be attributed to an increase in the fiber length. This hypothesis was confirmed by molecular weight measurements with SLS. Analysis of the molecular weight using a Zimm plot showed a dramatic decrease from 1.2 × 108 g/mol for **1**

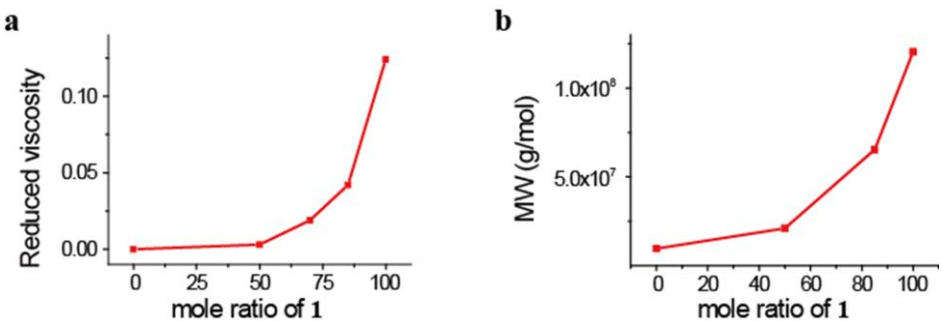

Figure 4. (a) Reduced viscosity and (b) absolute molecular weight (from SLS) as functions of the content of **1** (in mol %).

to 9.6 × 106 g/mol for **2**, and this trend is consistent with the viscosity results (Figure 4b). These results, together with the TEM data, demonstrate that the nanofiber length can be controlled by varying the **1**:**2** mole ratio.

The simultaneous presentation of mannose epitopes on a nanofiber scaffold

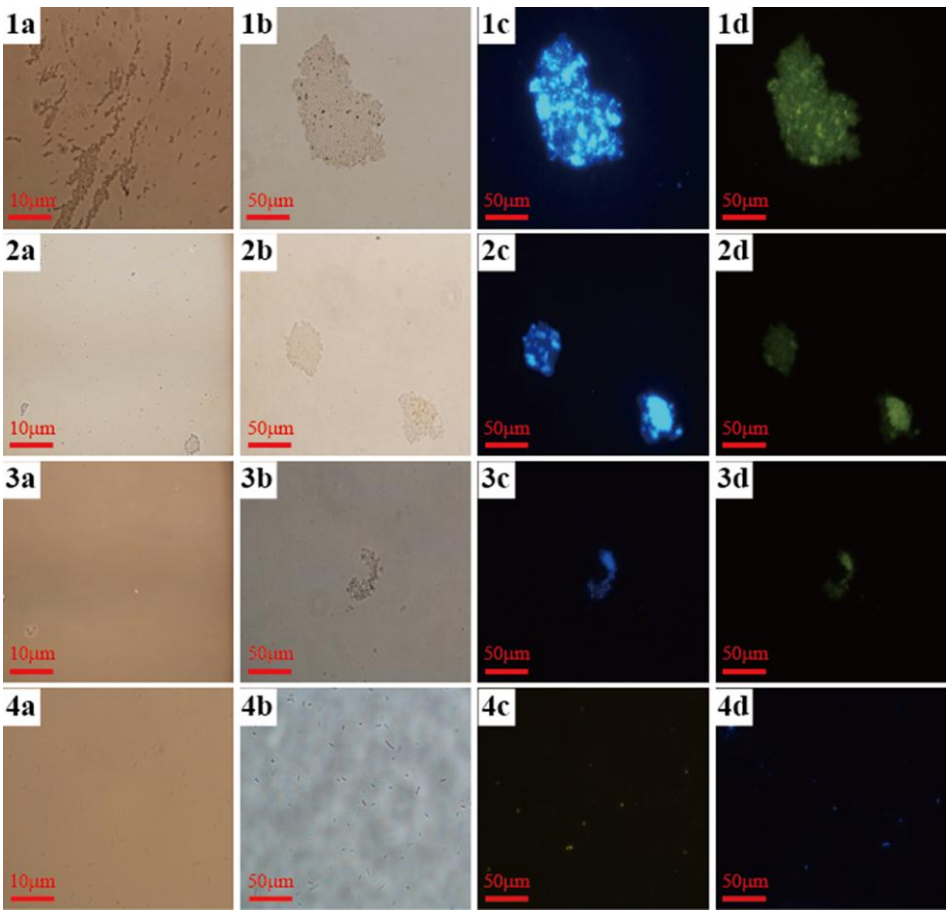

Figure 5. Microscope pictures, for exact fluorescence colocalization studies of the bacteria (yellow) with nanofiber (blue); (a) low magnification brightfield (10x), (b) bright field (50x), (c) fluorescence via excitation filter at 450-490 nm, (d) fluorescence via excitation filter at 340-380 nm. Incubation with (1) **1**, (2) **1**:**2** = 85:15, (3) **1**:**2** = 50:50, (4) **2**.

creates a multivalent ligand that has a high affinity for carbohydrate receptors.[19] For this reason, multivalent carbohydrate-coated molecules and nanofibers have been utilized as competitive inhibitors targeting several biological interactions.[20] Recent reports have shown that multivalent carbohydrate-coated nanofibers can induce agglutination and inhibit the motility of pathogenic cells.[21−23] To investigate the multivalent interactions between nanofibers and *Escherichia coli* cells, I choose an *E. coli* strain expressing the mannose-binding adhesion protein FimH in its type-1 pili (ORN 178 GFP). As shown in Figure 5, when the *E. coli* were incubated with pure **1** and with coassembled samples, clusters of fluorescent bacteria of different sizes were observed. The cluster size decreased with decreasing fiber length, indicating that the length of the mannose nanofibers plays a critical role in the agglutination of bacterial cells. In contrast, I did not observe bacterial agglutination with **2**, most likely because of the low aggregation stability of the fibers. To examine the ability of the nanofibers to agglutinate bacterial cells, agglutination index (AI) assays were performed (Figure 6a). Significant differences among the samples were observed in terms of the ability to agglutinate *E. coli*. The evaluated AI systematically increased with increasing **1** content. These results demonstrate that the length of the nanofibers has a significant influence on the formation of bacterial clusters and is a critical factor controlling agglutination. This result suggests that long nanofibers are able to aggregate *E. coli* cells dispersed in media, forming large bacterial clusters. However, the ability to aggregate *E. coli* decreases with decreasing fiber length.

Given adequate nutrition conditions and a pleasant environment, single-cell organisms such as *E. coli* can survive by proliferating, but uncontrolled bacterial proliferation is closely related to abnormal responses such as inflammation and

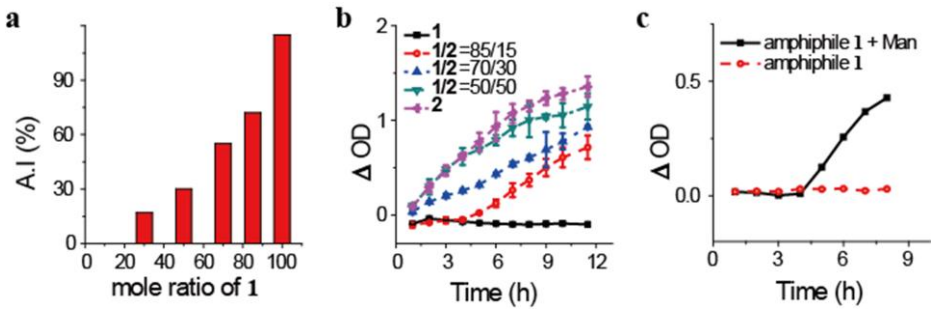

Figure 6. (a) Effect of the length of mannose-coated nanofibers on bacterial agglutination and proliferation. The degree of agglutination is represented by the agglutination index (AI). Each value represents the mean ± standard deviation (SD) of two independent experiments. (b) Growth curves based on the optical density (OD) at 600 nm for *E. coli* grown in the presence of **1**, **2**, and coassembled amphiphiles for 12 hours. Each value represents the mean ± SD of three independent experiments. (c) *E. coli* growth curves after addition of α-methyl-Dmannopyranoside.

autoimmune diseases. Therefore, the controlled proliferation of bacterial cells has emerged as an important issue. As previously reported.[2, 3, 7, 8] there is a close relationship between the form of bacterial clusters and the repression of the proliferation activity of bacteria cells. On the basis of these results, I anticipated that the length of the nanofibers would affect the size of the bacterial clusters and, subsequently, control bacteria proliferation. To confirm this hypothesis, I examined *E. coli* proliferation in the presence of mannose-coated nanofibers of different lengths. Spectrophotometric analysis based on turbidity or optical density (OD) is widely used to estimate the number of bacteria in liquid cultures.[24, 25] As the population of bacterial cells grows, the intensity of transmitted light decreases. As the first step in proliferation experiments, an overnight culture of *E. coli* strain

ORN 178 in Luria−Bertani (LB) medium was diluted in phosphate-buffered saline (PBS) until the OD at 600 nm (OD_{600}) was 1.1−1.2. The *E. coli* suspension was mixed with aliquots of **1**, **2**, and coassembled samples in PBS. I measured the variation in the size of the *E. coli* population by measuring OD_{600} every 30 min. As shown in Figure 6b, a normal bacterial growth curve was observed only in the presence of **2**. In contrast, I did not observe an increase in the cell population for **1** during our experimental time range. For the coassembled amphiphiles, the slope of the cell growth curve decreased with increasing **1** content. This result indicates that the proliferation of bacterial cells is regulated by the length of the carbohydrate-coated nanofibers, and this effect is attributed to the different agglutination forces for **1**, **2**, and the coassembled samples. This result indicates that the length of the nanofibers plays a critical role in regulating the proliferation of bacterial cells.

To determine whether this nanofiber is bacteriocidal or bacteriostatic, I added α-methyl-D-mannopyranoside (Man) as a specific competitor in high excess (1000-fold) to an agglutinated solution containing amphiphile **1** that had been incubated for 4 h. After the addition of excess Man, the bacterial cells started to proliferate, demonstrating that the agglutination was reversible (Figure 6c).

3. Conclusions

In summary, I was able to control the fiber length of carbohydrate-coated nanofibers by the coassembly of carbohydrate-conjugated rod amphiphiles with different aromatic segments. The major driving force controlling the length of the fibers is the level of crystallinity of the fiber cores. The resulting carbohydrate-coated nanofibers with controlled lengths can systematically regulate biological functions, such as the agglutination and proliferation of specific bacterial cells (Scheme 1).

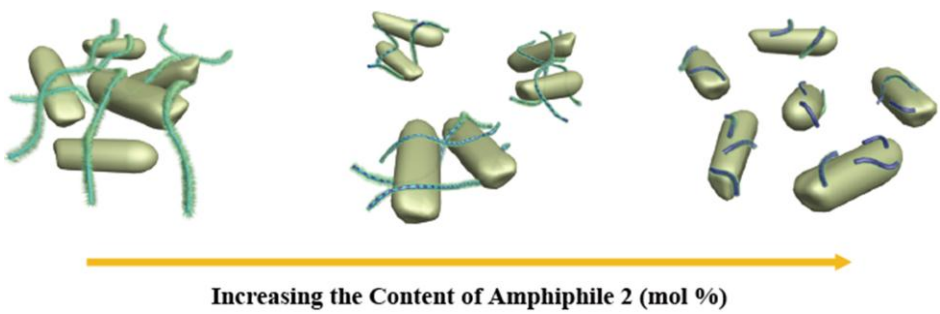

Scheme 1. Schematic representation of the regulation of agglutination and proliferation of bacterial cells by variation of the nanofiber length.

4. Experimental section

Materials

Tetrakis(triphenylphosphine) palladium(0), NaH(55 %), and *p*-toluenesulfonyl chloride (98 %) from TCI and Tokyo Kasei were used as received. 2,6-dibromophenol, 4-biphenylboronic acid, Pyrene-1-boronic acid, iodine monochloride (1.0 M solution in dichloromethane), boron tribromide (1.0 M solution in dichloromethane) from Aldrich were used as received. Unless otherwise indicated, all starting materials were obtained from commercial suppliers (Aldrich, Lancaster, and TCI, etc.) and were used without purification. Methylene chloride, hexane, Acetonitrile, DMF, and THF were distilled before use. Visualization was accomplished with UV light, iodine vapor or by staining using base solution of *p*-anisaldehyde. Flash chromatography was carried out with Silica Gel 60 (230-400 mesh) from EM Science.

Instruments

^{1}H-NMR was recorded from CDCl3 solutions on a Bruker AM 300 spectrometer. The purity of the products was checked by thin layer chromatography (TLC; Merck, silica gel 60). The UV/VIS absorption spectra were obtained from Hitachi U-2900. The fluorescence spectra were obtained from a Hithachi F-7000 Fluoresence Spectrophotometer. The transmission electron microscope (TEM) was performed at 120 kV using JEOL-JEM 2010. The 0.005% aqueous solution was dropped on carbon-coated copper grid and allowing the solution evaporates under ambient conditions. The bacteria agglutination was observed with a Nikon Eclipse TE2000-

U inverted fluorescence microscope equipped with a DXM1200C digital camera. Compounds were synthesized according to the procedure described scheme 2 and then purified by silica gel column chromatography and prep. HPLC (Japan Analytical Instrument). The SLS measurements were performed using a wide-angle light scattering photometer from ALV. The light source was a JDS Uniphase He-Ne laser (λ_0 = 632.8 nm, 35mW) emitting vertically polarized light. The cells were placed into the ALV/DLS/SLS-5000 Compact Goniometer System. The melting and crystallization behavior were evaluated using DSC Q2000 (TA, USA) with Autosampler and Mass Flow Control. MALDI TOF-MS spectroscopy (MALDI-TOF-MS) was performed on a Bruker Microflex LRF20 using α-cyano-4-hydroxy cinnamic acid (CHCA) as matrix.

Synthesis

Preparation of R-OTs: First–generation chiral dendritic tetraethylene glycol monobenzyl ether coils were prepared according to the similar procedures as described previously[26]. Then, hydrogenation of the dendritic coils over 20% Pd/C for 2 hours provided desire dendrimer. The crude mixture was filtered and concentrated in vacuum to yield 73% of a colorless liquid.

Synthesis of compound 4: Compounds **3**[27] (2 g, 4.0 mmol), **R-OTs** (2.9 g, 4.8 mmol) and excess K_2CO_3 were dissolved in 40 ml of distilled acetonitrile and DMF. The mixture was heated at reflux for 12 hours and then cooled to room temperature. After solvents were removed in a rotary evaporator, the mixture was extracted with ethyl acetate and water and then dried over anhydrous magnesium sulfate, and filtered. After the solvent was removed in a rotary evaporator, the crude products

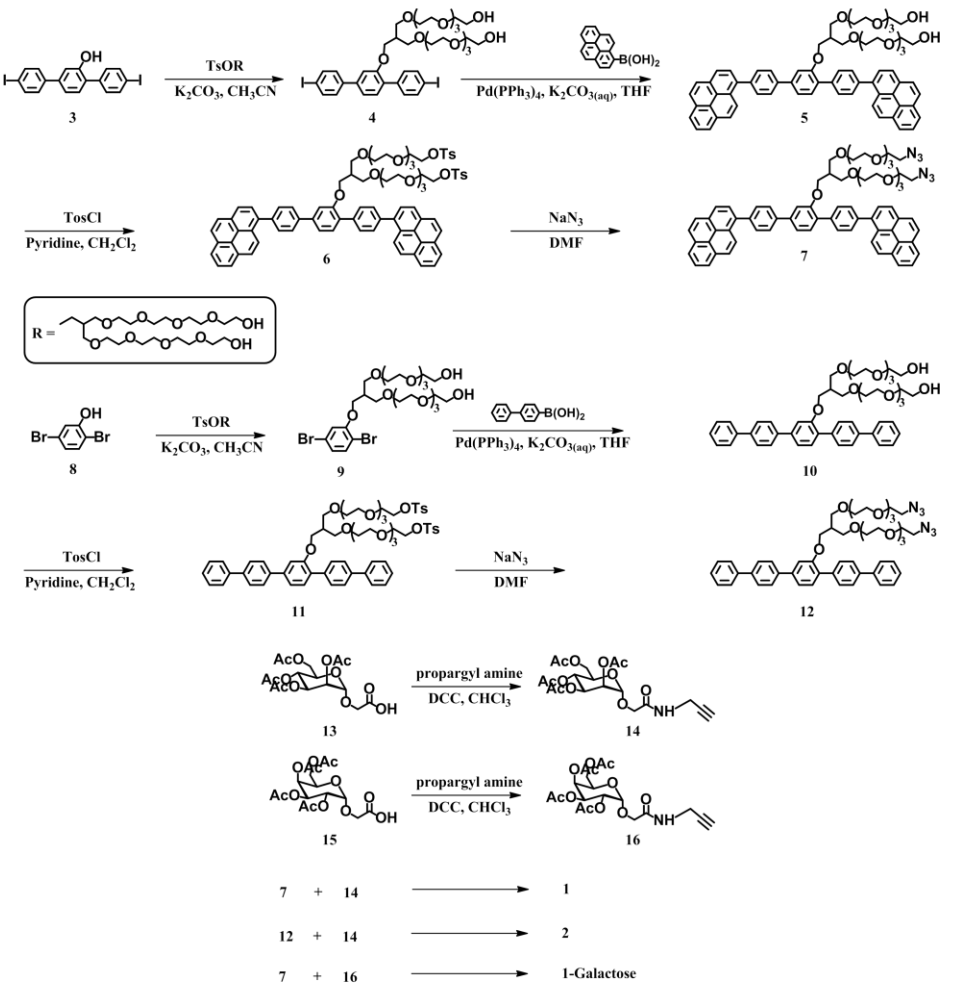

Scheme 2. A general outline of the synthetic procedure.

were purified by column chromatography (silica gel) using hexane : ethyl acetate (7 : 1 v/v) to yield 1.5 g (40 %) of a colorless liquid. ^{1}H-NMR (300 MHz, $CDCl_3$, δ, ppm) δ 7.79-7.72 (m, 4H, I-Ar-H), 7.38-7.32 (m, 4H, Ar-H), 7.28 (s, 2H, Ar-H), 7.18 (s, 1H, Ar-H) 4.12 (s, 2H, -C*H*$_2$OAr), 3.65-3.48(m, 36H; -C*H*$_2$O), 2.66 (s, 2H; -OH), 2.55-2.53 (m, 1H;-CH_2C*H*CH_2O-); ^{13}C-NMR (75.5 MHz, $CDCl_3$, δ, ppm) δ 156.5, 141.4, 140.6, 138.2, 138.0, 137.3, 131.8, 131.2, 129.3, 119.7, 111.4, 72.6,

70.6, 70.5, 70.4, 70.3, 69.0, 67.2, 61.7, 39.8; MALDI-TOF-MS [MH]+ calcd. for $C_{38}H_{52}I_2O_{11}$: m/z : 938.16; Found: 961.1 [M+Na^+].

Synthesis of compound 5: Compound **4** (1.3 g, 1.4 mmol) and 1-pyrenylboronic acid (0.75 g, 3 mmol) were dissolved in 30 ml THF and added 40 ml of degassed 2.0 M Na_2CO_3 aqueous solution. Then tetrakis(triphenylphosphine) palladium(0) (0.1 g, 0.1 mmol) was added. The mixture was heated at reflux for 24 hours with vigorous stirring under nitrogen. Cooled to room temperature, the layers were separated, and the aqueous layer was then washed twice with ethyl acetate. The combined organic layer was dried over anhydrous magnesium sulfate and filtered. The solvent was removed in a rotary evaporator, and the crude product was purified by column chromatography (silica gel) using hexane : ethyl acetate (10 : 1 v/v) as eluent to yield 1.2 g (78 %) of yellow liquid. ^{1}H-NMR (300 MHz, $CDCl_3$, δ, ppm) δ 8.30-7.45(m, 29H, pyrene-Ar-H), 4.13 (s, 2H, -C*H*$_2$OAr), 3.65-3.48(m, 36H; -C*H*$_2$O), 2.65 (s, 2H; -OH), 2.55-2.53 (m, 1H;-CH_2C*H*CH_2O-); ^{13}C-NMR (75.5 MHz, $CDCl_3$, δ, ppm) δ 132.3, 132.2, 132.1, 132.0, 131.7, 131.2, 130.3, 129.8, 128.7, 128.6, 127.7, 127.66, 127.6, 127.3, 125.0, 124.8, 72.6, 70.6, 70.5, 70.4, 70.3, 69.0, 67.2, 61.7, 39.8; MALDI-TOF-MS [MH]+ calcd. for $C_{70}H_{70}O_{11}$: m/z: 1087.49; Found: 1110.4 [M+Na^+].

Synthesis of compound 6: Compound **5** (1 g, 0.92 mmol) and p-tolunesulfonic chloride (0.4 g, 2 mmol) were dissolved in 30 ml dried methylene chloride and added 40 ml of pyridine. The mixture was stirred over 12 hours with vigorous stirring under nitrogen. The resulting mixture was extracted with ethyl acetate and water. The crude product was dried over anhydrous magnesium sulfate, and filtered. The solvent was removed in a rotary evaporator, and the crude product was

purified by column chromatography (silica gel) using hexane : ethyl acetate (10 : 1 v/v) as eluent to yield 0.6 g (47 %) of liquid. ^{1}H-NMR (300 MHz, $CDCl_3$, δ, ppm) δ 8.30-7.70(m, 37H, pyrene-Ar-Tosyl Ar-H), 4.13 (s, 2H, -C*H*$_2$OAr), 4.09-4.04 (t, 4H; -C*H*$_2$O-Tosyl) 3.65-3.48 (m, 32H; -C*H*$_2$O), 2.55-2.53 (m, 1H;-CH_2C*H*CH_2O-), 2.36 (s, 6H; CH_3-Tosyl),; ^{13}C-NMR (75.5 MHz, $CDCl_3$, δ, ppm) δ 144.7, 132.9, 132.3, 132.2, 132.1, 132.0, 131.7, 131.2, 130.3, 129.8, 129.7, 128.7, 128.6, 127.9, 127.7, 127.66, 127.6, 127.3, 125.0, 124.8, 72.9, 70.93, 70.93, 70.73, 70.61, 69.65, 66.90, 60.2; MALDI-TOF-MS [MH]+ calcd. for $C_{84}H_{82}O_{15}S_2$: m/z: 1394.51; Found: 1417.3 [M+Na^+].

Synthesis of compound 7: Compound **6** (0.6 g, 0.43 mmol) and sodium azide (0.11 g, 1.72 mmol) were dissolved in 30 ml dried DMF. The mixture was stirred over 6 hours with vigorous stirring under nitrogen. After the solvent was removed in a rotary evaporator, the crude products were purified by column chromatography (silica gel) using hexane : ethyl acetate (7 : 1 v/v) to yield 0.35 g (71 %) of a colorless liquid., ^{1}H-NMR (300 MHz, $CDCl_3$, δ, ppm) δ 8.30-7.45(m, 29H, pyrene-Ar-H), 4.13 (s, 2H, -C*H*$_2$OAr), 3.65-3.48(m, 32H; -C*H*$_2$O), 3.28(s, 4H; -CH_2C*H*$_2$-N_3), 2.55-2.53 (m, 1H;-CH_2C*H*CH_2O-); ^{13}C-NMR (75.5 MHz, $CDCl_3$, δ, ppm) δ 132.3, 132.2, 132.1, 132.0, 131.7, 131.2, 130.3, 129.8, 128.7, 128.6, 127.7, 127.66, 127.6, 127.3, 125.0, 124.8, 72.9, 70.93, 70.93, 70.73, 70.61, 69.65, 66.90, 50.6; MALDI-TOF-MS [MH]+ calcd. for $C_{70}H_{68}N_6O_9$: m/z: 1136.50; Found: 1159.5 [M+Na^+].

Synthesis of compound 8: This compound was synthesized using the same procedure from compound **4**. ^{1}H-NMR (300 MHz, $CDCl_3$, δ, ppm) δ 7.32-7.28 (d, 1H, Ar-H), 7.03-7.01 (d, 1H; Ar-H), 6.92-6.89 (d, 1H; Ar-H), 4.11-4.08 (d, 2H; -

C*H*$_2$OAr), 3.75-3.54 (m, 36H; -C*H*$_2$O), 2.66 (s, 2H; -OH), 2.55-2.53 (m, 1H; -CH$_2$C*H*CH$_2$O); ^{13}C-NMR (75.5 MHz, CDCl$_3$, δ, ppm) δ 156.0, 133.9, 124.6, 121.5, 116.6, 110.9, 72.6, 70.6, 70.5, 70.4, 70.3, 69.0, 67.2, 61.7, 39.8; MALDI-TOF-MS [MH]+ calcd. for $C_{26}H_{44}Br_2O_{11}$: m/z: 692.12; Found: 715.1 [M+Na$^+$].

Synthesis of compound 10: This compound was synthesized using the same procedure from compound **5**. ^{1}H-NMR (300 MHz, CDCl$_3$, δ, ppm) δ 7.78-7.66 (m, 12H; Ar-H), 7.50-7.45 (m, 5H; Ar-H), 7.40-7.30 (m, 4H; Ar-H), 4.21-4.17 (d, 2H; -C*H*$_2$OAr), 3.75-3.48(m, 36H; -C*H*$_2$O), 2.68 (s, 2H; -OH), 2.55-2.53 (m, 1H; -CH$_2$C*H*CH$_2$O-); ^{13}C-NMR (75.5 MHz, CDCl$_3$, δ, ppm) δ 131.0, 130.2, 129.9, 128.5, 128.4, 127.8, 127.79, 127.4, 124.4, 72.6, 70.6, 70.5, 70.4, 70.3, 69.0, 67.2, 61.7, 39.8; MALDI-TOF-MS [MH]+ calcd. for $C_{50}H_{62}O_{11}$: m/z: 838.43; Found: 861.4 [M+Na$^+$].

Synthesis of compound 11: This compound was synthesized using the same procedure from compound **6**. ^{1}H-NMR (300 MHz, CDCl$_3$, δ, ppm) δ 7.79-7.61 (m, 16H; Ph Ar-Tosyl Ar-H), 7.50-7.44 (m, 5H; Ph Ar-H), 7.38-7.25 (m, 8H; Ph Ar-Tosyl Ar-H), 4.16-4.13 (d, 2H; -C*H*$_2$OAr), 4.09-4.04 (t, 4H; -C*H*$_2$O-Tosyl), 3.71-3.51 (m, 32H; -C*H*$_2$O), 2.55-2.53 (m, 1H; -CH$_2$C*H*CH$_2$O-), 2.38(s, 6H; CH$_3$-Tosyl); ^{13}C-NMR (75.5 MHz, CDCl$_3$, δ, ppm) δ 144.7, 132.9, 131.0, 130.2, 129.9, 129.7, 128.5, 128.4, 127.86, 127.8, 127.79, 127.4, 124.4, 72.9, 70.93, 70.93, 70.73, 70.61, 69.65, 66.90, 60.2; MALDI-TOF-MS [MH]+ calcd. for $C_{64}H_{74}O_{15}S_2$: m/z: 1146.45; Found: 1169.4 [M+Na$^+$].

Synthesis of compound 12: This compound was synthesized using the same procedure from compound **7**. ^{1}H-NMR (300 MHz, CDCl$_3$, δ, ppm) δ 7.76-7.65 (m,

12H; Ar-H), 7.50-7.45 (m, 5H; Ar-H), 7.40-7.31 (m, 4H; Ar-H), 4.21-4.17 (d, 2H; -C*H*$_2$OAr), 3.65-3.48 (m, 32H; -C*H*$_2$O), 3.28 (s, 4H; -CH$_2$C*H*$_2$-N$_3$), 2.55-2.53 (m, 1H; -CH$_2$C*H*CH$_2$O-); ^{13}C-NMR (75.5 MHz, $CDCl_3$, δ, ppm) δ 131.0, 130.2, 129.9, 128.5, 128.4, 127.8, 127.79, 127.4, 124.4, 72.9, 70.93, 70.93, 70.73, 70.61, 69.65, 66.90, 50.6; MALDI-TOF-MS [MH]+ calcd. for $C_{50}H_{60}N_6O_9$: m/z: 888.44; Found: 911.4 [M+Na$^+$].

Synthesis of compound 14: Compound **13**[28] (0.3 g, 0.74 mmol) were dissolved in dry CH_2Cl_2 (10 mL) and added DCC and catalytic amount of DMAP at 0℃. After 30min, the reagent mixture was added 4-nitrophenol (54 mg, 0.39 mmol), and the resulting mixture was stirred vigorously for 8 hours at room temperature. Propargyl amine (0.1 ml) was added and the resulting mixture was stirred at room temperature for another 6 hrs. After that the solvent was removed in a rotary evaporator, the crude products were purified by column chromatography (silica gel) using hexane : ethyl acetate (1 : 1 v/v) to yield 0.17 g (52 %) of a colorless liquid. ^{1}H-NMR (300 MHz, $CDCl_3$, δ, ppm) δ 5.62-5.61 (d, 1H; -(CH)OC*H*O-), 5.59-5.19 (m, 3H, -AcOC*H*-), 4.48-4.05 (m, 5H; -AcOC*H*$_2$CH-, -OC*H*$_2$CO-, -CH$_2$CH-), 2.27 (t, 2H, -CCH$_2$NH-), 2.21-2.00 (m, 12H; -*H*$_3$CCO), 1.82 (s, 1H; -*CHC*-); ^{13}C-NMR (75.5 MHz, $CDCl_3$, δ, ppm) δ 170.4, 170.2, 170.1, 170.0, 169.99, 169.93, 169.9, 168.3, 168.2, 101.2, 101.0, 98.2, 79.2, 72.0, 71.8, 71.7, 71.1, 70.9, 70.8, 70.6, 70.4, 68.9, 68.7, 68.5, 67.1, 66.9, 61.3, 28.59; MALDI-TOF-MS [MH]+ calcd. for $C_{19}H_{25}NO_{11}$: m/z: 443.14; Found: 466.1 [M+Na$^+$].

Synthesis of compound 16: This compound was synthesized using the same procedure from compound **14**. ^{1}H-NMR (300 MHz, $CDCl_3$, δ, ppm) δ 5.39-5.37 (d, 1H; -(CH)OC*H*O-), 5.27-5.23 (m, 1H, -AcOC*H*-), 5.07-5.02 (m, 1H, -AcOC*H*-),

4.62-4.60 (m, 1H, -AcOC*H*-), 4.35-4.07 (m, 5H; -AcOCH_2CH-, -OCH_2CO-, -CH_2CH-), 2.27 (t, 2H, -CCH_2NH-), 2.21-2.00 (m, 12H; -H_3CCO), 1.82 (s, 1H; -*CHC*-); ^{13}C-NMR (75.5 MHz, $CDCl_3$, δ, ppm) δ 170.4, 170.2, 170.1, 170.0, 169.99, 169.93, 169.9, 168.3, 168.2, 101.2, 101.0, 98.2, 79.2, 72.0, 71.8, 71.7, 71.1, 70.9, 70.8, 70.6, 70.4, 68.9, 68.7, 68.5, 67.1, 66.9, 61.3, 28.59; MALDI-TOF-MS [MH]+ calcd. for $C_{19}H_{25}NO_{11}$: m/z: 443.14; Found: 466.1 [M+Na^+].

Synthesis of compound 1, 2, 1-Galactose: A solution of compound azido amphiphiles (**7, 12)** and propargylated carbohydrate (**14, 16**) in THF with catalytic amouns of sodium-ascorbate (5 mol%) and $CuSO_4$ (2 mol%) was stirred at RT for 2 hours. The solution color was changed from orange to green. After the solvent was removed in a rotary evaporator, diluted with chroloform and then extracted with water two times. The organic layer was dried over anhydrous magnesium sulfate and filtered. The solvent was removed in a rotary evaporator. The crude product was purified by silica gel column chromatography (silica gel, CH_2Cl_2 : MeOH = 10 : 1) and prep. HPLC (Japan Analytical Instrument) to yield 120 mg (60 %). Finally acetyl blocked compounds dissolved in MeOH/THF mixture solvent and added NaOMe. The resulting mixture was stirred vigorously for 30 min and the solvent was removed in a rotary evaporator.

Componud 1 : ^{1}H-NMR (300 MHz, DMSO, δ, ppm) δ 8.57-7.62(m, 29H, pyrene-Ar-H), 4.85-4.68 (d, 2H; -(CH)OC*H*O-, 2H, -CH_2N*H*CO-, 8H; -NHCH_2C- and –OCCH_2O-), 4.43-4.00 (m, 14H; HOCH_2C-, HOCH$(CH)_2$-, -CH_2CH$(CH)_2$-, -$(CH)_2$CHO-), 3.74-3.73 (d, 2H; -CH_2OAr), 3.74-3.30 (m, 36H; -OCH_2CH_2, contain DMSO solvent H_2O peak); ^{13}C-NMR (75.5 MHz, DMSO, δ, ppm) δ 170.3, 167.6, 157.3, 145.7, 140.1, 132.3, 132.2, 131.7, 131.5, 131.2, 130.8, 128.9, 128.7, 128.3,

127.7, 126.3, 125.5, 125.3, 124.4, 105.1, 76.7, 74.2, 71.8, 71.3, 71.0, 70.9, 70.8, 70.7, 70.6, 69.8, 69.3, 69.1, 61.6, 50.5, 35.1; MALDI-TOF-MS [MH]+ calcd. for $C_{92}H_{102}N_8O_{23}$: m/z 1687.71; Found: 1710.7 [M+Na^+].

Componud 2 : ^{1}H-NMR (300 MHz, DMSO, δ, ppm) δ 8.48-8.41 (m, 6H; Ar-H), 7.88-7.39 (m, 15H; Ar-H), 4.85-4.65 (d, 2H; -(CH)OC*H*O-, s, 2H, -CH_2NHCO-, m, 8H; -NHCH_2C- and –OCCH_2O-), 4.44-4.00 (m, 14H; HOCH_2C-, HOCH(CH)$_2$-, -CH_2CH(CH)$_2$-, -(CH)$_2$CHO-), 4.11-4.08 (d, 2H; -CH_2OAr), 3.74-3.36 (m, 36H; -OCH_2CH_2, contain DMSO solvent H_2O peak); ^{13}C-NMR (75.5 MHz, DMSO, δ, ppm) δ 170.3, 167.6, 157.3, 145.7, 141.6, 131.0, 130.2, 129.9, 128.5, 128.4, 127.8, 127.7, 127.4, 124.4, 105.1, 76.7, 74.2, 71.8, 71.1, 71.0, 70.9, 70.8, 70.7, 70.6, 69.9, 69.3, 69.1, 61.6, 50.5, 35.1; MALDI-TOF-MS [MH]+ calcd. for $C_{72}H_{94}N_8O_{23}$: m/z 1438.6; Found: 1462.4 [M+Na^+].

Componud 1-Galactose : ^{1}H-NMR (300 MHz, DMSO, δ, ppm) δ 8.57-7.62(m, 29H, pyrene-Ar-H), 4.79-4.62 (d, 2H; -(CH)OC*H*O-, 2H, -CH_2N*H*CO-, 8H; -NHC*H*$_2$C- and –OCC*H*$_2$O-), 4.51-3.97 (m, 14H; HOCH_2C-, HOCH(CH)$_2$-, -CH_2CH(CH)$_2$-, -(CH)$_2$CHO-), 3.74-3.73 (d, 2H; -CH_2OAr), 3.74-3.30 (m, 36H; -OCH_2CH_2, contain DMSO solvent H_2O peak); ^{13}C-NMR (75.5 MHz, DMSO, δ, ppm) δ 170.3, 167.6, 157.3, 145.7, 140.1, 132.3, 132.2, 131.7, 131.5, 131.2, 130.8, 128.9, 128.7, 128.3, 127.7, 126.3, 125.5, 125.3, 124.4, 105.1, 76.7, 74.2, 71.8, 71.3, 71.0, 70.9, 70.8, 70.7, 70.6, 69.8, 69.3, 69.1, 61.6, 50.5, 35.1; MALDI-TOF-MS [MH]+ calcd. for $C_{92}H_{102}N_8O_{23}$: m/z 1687.71; Found: 1710.7 [M+Na^+].

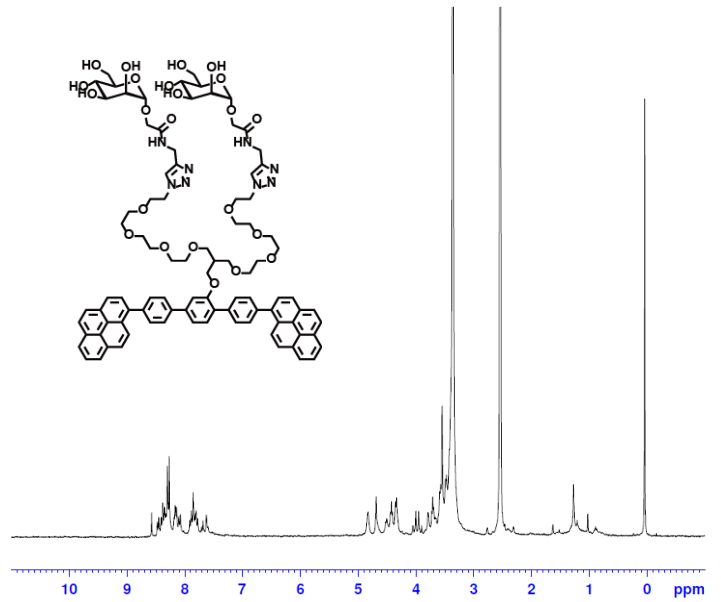

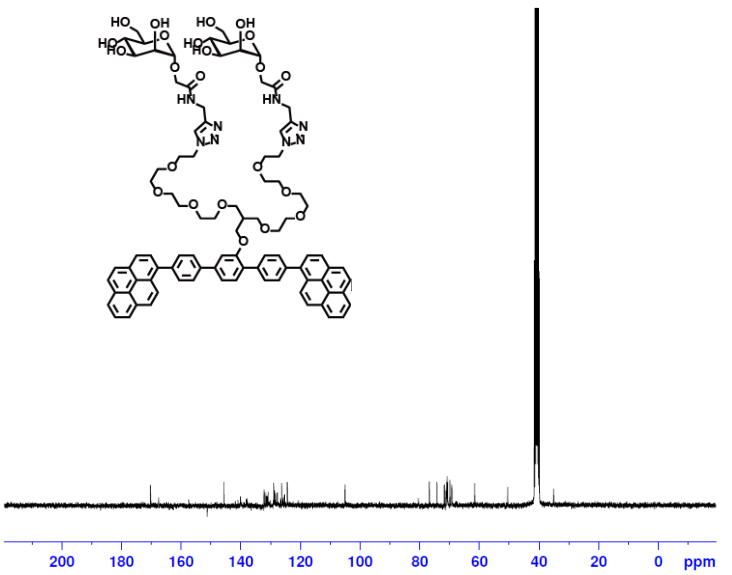

Figure 7. (a) ^{1}H (b) ^{13}C NMR spectra of amphiphile **1**

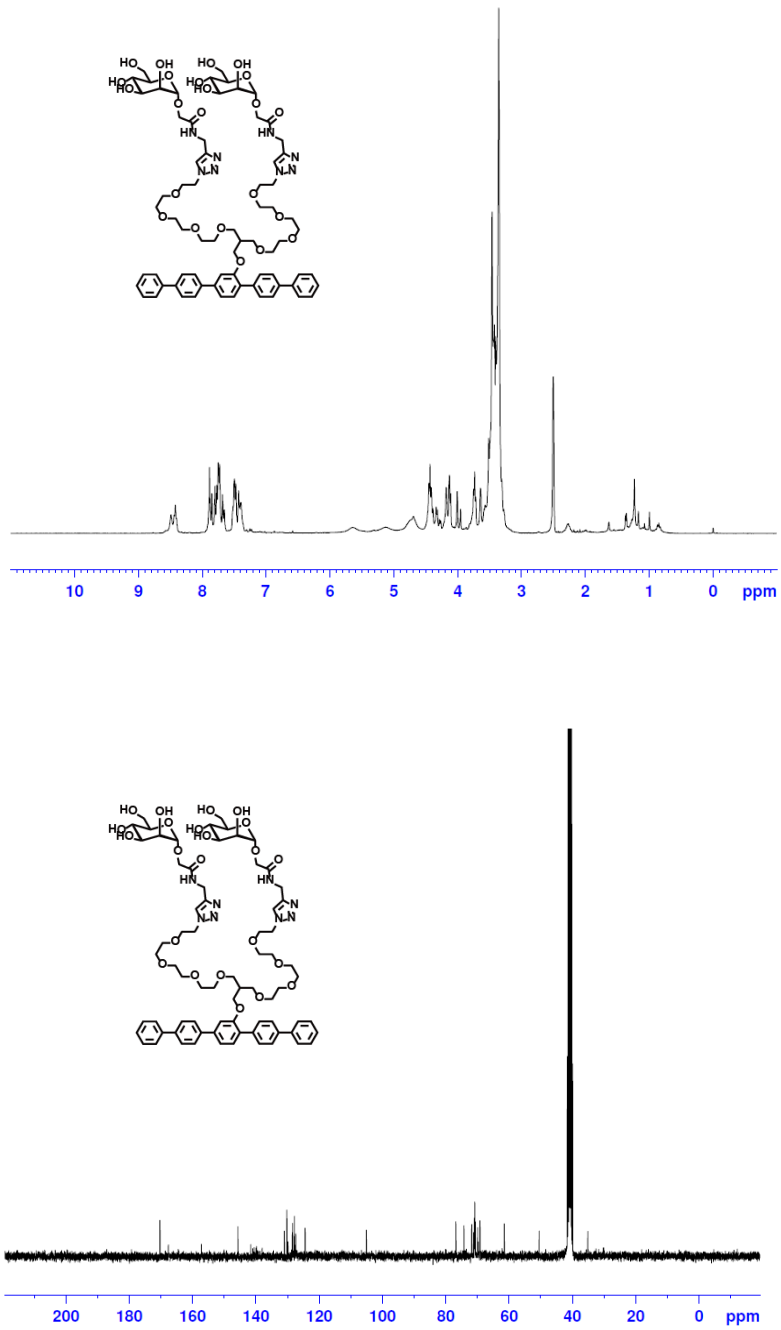

Figure 8. (a) ^{1}H (b) ^{13}C NMR spectra of amphiphile **2**

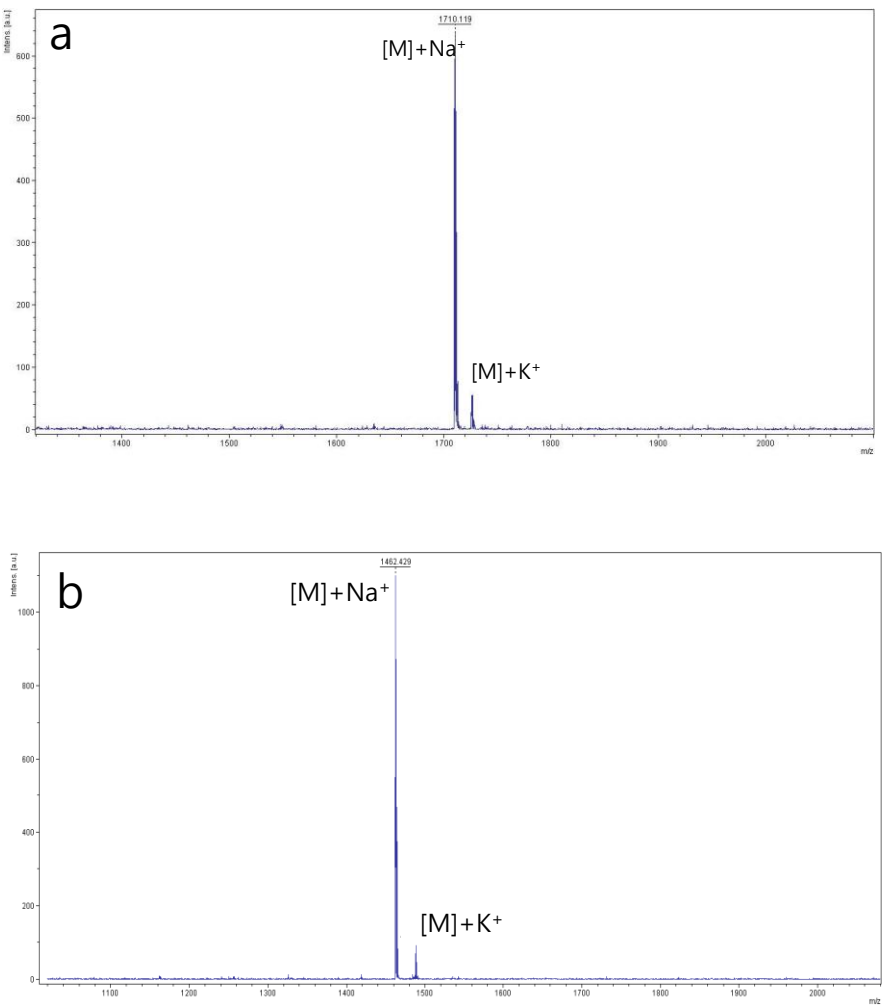

Figure 9. MALDI-TOF mass spectra a) amphiphile **1**, b) amphiphile **2**

Methods

Fiber Generation and TEM sample preparation: 60 μM of amphiphiles was dissolved in 1mL pure water in 3 mL vial and placed in a water bath at room temperature with mild sonication. After 2 hours, the aqueous solution was slowly dropped on a carbon-coated copper grid and the solution was allowed to evaporate under RT. The samples were stained by depositing a drop of uranyl acetate onto the surface of the sample-loaded grid then dried at RT.

Differential scanning calorimetry (DSC) Measurement: The melting and crystallization behavior were evaluated using DSC Q2000 and scanned at a heating and cooling rate of 10℃ min^{-1} in nitrogen atmosphere. Samples weighing about 3~4 mg were used for this measurement.

The Viscosity and Static Light Scattering (SLS) measurement: The reduced viscosity was measured at concentration of about **2**, 1.5, 1, 0.5 mg/ml of solvent by determining the flow time of a certain volume of solution through a capillary of fixed length. Flow time in second is recorded as the time for the meniscus to pass between two designated marks on the viscometer. Viscosities were run at constant temperature, usually 25 ℃. The SLS measurements were performed using a wide-angle light scattering photometer from ALV. The light source was a JDS Uniphase He-Ne laser (λ_0 = 632.8 nm, 35 mW) emitting vertically polarized light. The cells were placed into the ALV/DLS/SLS-5000 Compact Goniometer System. All measurement was carried out at room temperature. SLS experiments were performed simultaneously. The scattering angular range is between 20^o and 150^o (at 5^o interval) and toluene was used as the standard in the SLS measurement. The SLS

experiments were carried on solution of amphiphile **1**, **2** and co-assembled samples in water at four different concentration (c = 2, 1.5, 1, 0.5 mg/mL) for each sample.

***E.coli* Microscopy Experiment**: 0.2 ml frozen culture of *E. coli* stains ORN 178 GFP was grown overnight in 5ml LB media with Tetracycline (4 mg/mL) and Ampicilin (0.1 mg/ml) in an incubater (37 ℃) with shaking. The *E. coli* culture was diluted to reach an OD_{600} to 1. The bacterial culture was centrifuged for 3 min at 13000rpm. The liquid was removed and the bacteria pellet re-suspended in 1 ml of PBS buffer and washed two times with same buffer. Finally, the bacterial pellet was re-suspended in 1 ml PBS buffer and added (20 μl) amphiphile **1**, **2** and one of co-assembled samples which was dissolved in PBS buffer. This mixture solution was incubated for 2 hours at (37 ℃) and this suspension was fixed on microscope slides, covered with glass slides for checking fluorescence co-localization studies of the bacteria with compounds.

***E. coli* Agglutination Index Assay**: The *E. coli* was observed with a Nikon Eclipse TE-2000U inverted fluorescence microscope equipped with a DXM1200C digital camera. The agglutination index (AI) was calculated from 10 random fields of microscopic images (929 μm x 690 μm), where the number of cells in close contact were counted and averaged.

***E. coli* Proliferation Assay**: The OD600 was measured and diluted with LB media to reach an OD600 of 1.1~1.2. After taking 1 ml of bacterial culture to eppendorf tube, centrifuged for 3 min at 13000 rpm. The LB media liquid was removed and white bacteria pellet was re-suspended in 1 ml PBS buffer solution. This solution (10 μl) was added to each co-assembled amphiphiles solution (1 mg + 490 μl LB

media) and all samples were put into incubater (37 ℃) with mild shaking. The OD600 of each samples was measured at every 30 min.

Supporting Figures

Comparison study between amphiphile 1-Mannose and 1-Galactose

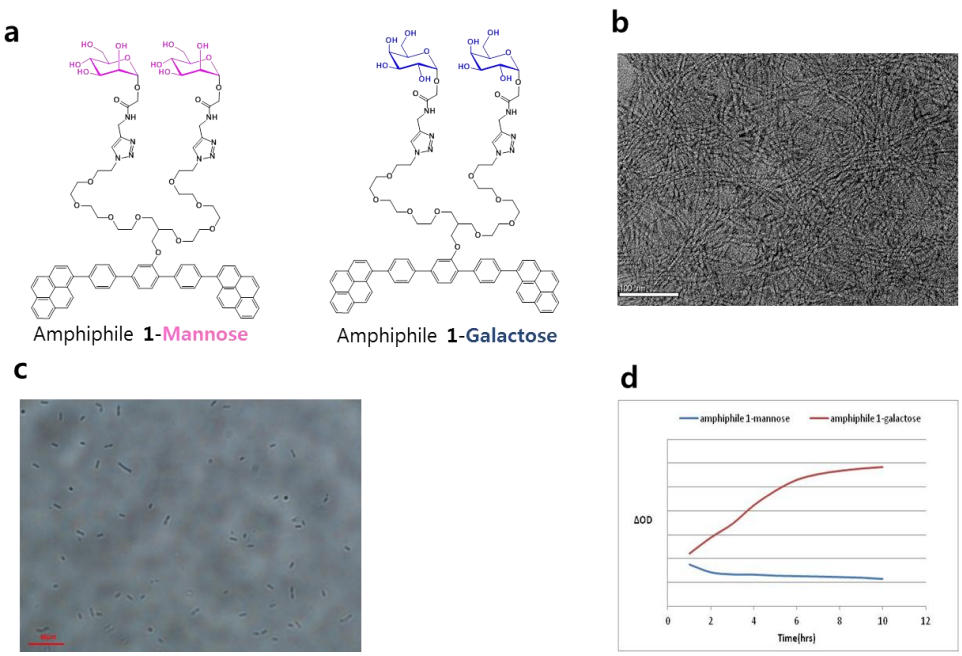

Figure 10. a) Amphiphile **1**-Mannose and **1**-Galactose chemical structure, b) TEM image of **1**-Galactose (60 μM), c) Microscope pictures (bright field) after incubation with **1**-Galactose and bacteria (ORN 178), d) *E. coli* growth curve with **1**-Galactose.

E. coli (ORN 208) Growth curve with Nanofibers

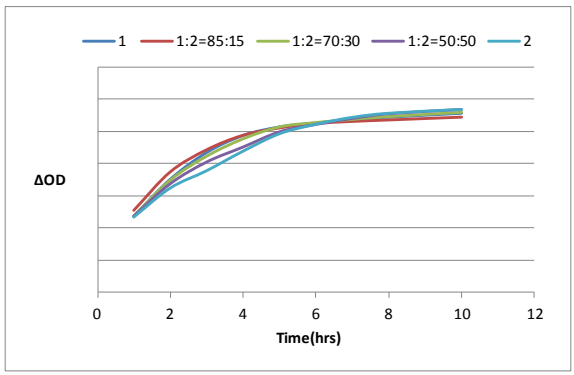

Figure 11. Growth curve of ORN 208 with mannose-coated nanofibers.

5. References

(1) Müller, M. K.; Brunsveld, L. *Angew. Chem. Int. Ed.* **2009**, *48*, 2921.

(2) Lim, Y.; Park, S.; Lee, E.; Ryu, J. H.; Yoon, Y. R.; Kim, T. H.; Lee, M. *Chem. -Asian. J.* **2007**, *2*, 1363.

(3) Lim, Y.; Park, S.; Lee, E.; Jeong, H.; Ryu, J. H.; Lee, M. S.; Lee, M. *Biomacromolecules* **2007**, *8*, 1404.

(4) Dolphin, G. T.; Dumy, P.; Garcia, J. *Angew. Chem. Int. Ed.* **2006**, *45*, 2699.

(5) Baldwin, A. J.; Bader, R.; Christodoulou, J.; MacPhee, C. E.; Dobson, C. M.; Barker, P. D. *J. Am. Chem. Soc.* **2006**, *128*, 2162.

(6) Hentschel, J.; Krause, E.; Börner, H. G. *J. Am. Chem. Soc.* **2006**, *128*, 7722.

(7) Wang, H.; Gu, L.; Lin, Y.; Lu, F.; Meziani, M. J.; Luo, P. G.; Wang, W.; Cao, L.; Sun, Y. P. *J. Am. Chem. Soc.* **2006**, *128*, 13364.

(8) Luo, P. G.; Wang, H.; Gu, L.; Lu, F.; Lin, Y.; Christensen, K. A.; Yang, S. T.; Sun, Y. P. *ACS nano* **2009**, *3*, 3909.

(9) Gregorio, C. C.; Weber, A.; Bondad, M.; Pennise, C. R.; Fowler, V. M. *Nature* **1995**, *377*, 83.

(10) Gestwicki, J. E.; Christopher, W.; Strong, L. E.; Oetjen, K. A.; Kiessling, L. L. *J. Am. Chem. Soc.* **2002**, *124*, 14922.

(11) Wang, X.; Guerin, G.; Wang, H.; Wang, Y.; Manners, I.; Winnik, M. A. *Science* **2007**, *317*, 644.

(12) Guérin, G.; Wang, H.; Manners, I.; Winnik, M. A. *J. Am. Chem. Soc.* **2008**, *130*, 14763.

(13) Gilroy, J. B.; Gädt, T.; Whittell, G. R.; Chabanne, L.; Mitchels, J. M.; Richardson, R. M.; Winnik, M. A.; Manners, I. *Nature chem.* **2010**, *2*, 566.

(14) Besenius, P.; Portale, G.; Bomans, Paul H. H.; Janssen, H. M.; Palmans, Anja R. A; Meijer, E. W. *Proc. Natl. Acad. Sci. USA.* **2010**, *107*, 17888

(15) Steve, R.; Palmer, L. C.; Fry, N. J.; Greenfield, M. A.; Messmore, B. W.; Meade, T. J.; Stupp, S. I. *J. Am. Chem. Soc.* **2008**, *130*, 2742.

(16) Moon, K.-S.; Kim, H.-J.; Lee, E.; Lee, M. *Angew. Chem. Int. Ed*. **2007**, *46*, 6807.

(17) Lee, E.; Kim, J.-K.; Lee, M. *Angew. Chem. Int. Ed*. **2008**, *47*, 6375.

(18) Huang, Z.; Lee, H.; Lee, E.; Kang, S.-K.; Nam, J.-M.; Lee, M. *Nature Commun*. **2011**, *2*, 459.

(19) Mark L. Wolfenden; Mary J. Cloninger. *J. Am. Chem. Soc.* **2005**, *127*, 12168

(20) Mammen, M.; Choi, S.-K.; Whitesides, G. M. *Angew. Chem. Int. Ed.* **1998**, *37*, 2754

(21) Ryu, J.-H.; Lee, E.; Lim, Y.-b.; Lee, M. *J. Am. Chem. Soc.* **2007**, *129*, 4808.

(22) Gestwicki, J. E.; Strong, L. E.; Cairo, C. W.; Boehm, F. J.; Kiessling, L. L. *Chem.&Biol. J.* **2002**, *9*, 163.

(23) Gu, L.; Elkin, T.; Jiang, X.; Li, H.; Lin, Y.; Qu, L.; Tzeng, T.-R. J.; Joseph, R.; Sun, Y.-P. *Chem. Commun.* **2005**, 874.

(24) Wang, B.; Liu, P.; Jiang, W.; Pan, H.; Xu, X.; Tang, R. *Angew. Chem. Int. Ed.* **2008**, *47*, 3560.

(25) Kim, J.; Ahn, Y.; Park, K. M.; Lee, D.-W.; Kim, K. *Chem.-Eur. J.* **2010**, *16*, 12168.

(26) Jayaraman, M.; Fréchet, J. M. J. *J. Am. Chem. Soc.* **1998**, *120*, 12996.

(27) D.-W. Lee, Taehoon, Kim, M. Lee. *Chem. Commun.* **2011**, *47*, 8529

(28) Y-b. Lim; M. Lee et al. *Biomacromolecules* **2007**, *8*, 1404

국문 초록

다중 리간드 역할을 하는 초분자 나노섬유의 박테리아 응집 조절

김태훈
화학부 유기화학전공
서울대학교 대학원

수용액상에서 자기 조립된 나노구조체의 크기와 모양을 조절하는 것은 생체 기능을 조절하는데 매우 중요하다. 또한 잘 디자인된 유기 분자가 이루는 초분자 구조체 중 1차원의 나노 섬유는 생체 친화적인 물질로써 그 응용 가능성이 높아 여러 분야에서 연구주제로 큰 관심을 받고 있다. 자기 조립을 통하여 나노섬유를 제조하는 것은 다양한 기술과 방법을 통해 가능하지만 그 섬유의 길이를 조절하는 데는 아직 한계가 있다. 본 연구는 파이-파이 쌓임 상호작용 (π–π stacking interactions) 이 조절되도록 서로 다른 결정성을 갖는 방향족 로드와 친수성 코일로 이루어진 양친매성 분자를 다양한 비율로 함께 자기 조립하여 만들어진 섬유의 길이를 조절하는 한계를 극복하고자 한다. 더불어 분자의 끝에 탄수화물 기능기를 도입하여 자기 조립된 섬유가 박테리아 세포에 달라붙을 수 있게 하였다. 특히, 이러한 섬유의 체계적인 길이 조절은 섬유에게 노출된 박테리아 세포의 응집과 성장을 조절하는 특징을 나타낸다.

주요어 : 다중 리간드, 탄수화물로 코팅된 나노섬유, 자기조립, 길이 조절, 박테리아 응집, 박테리아 세포 성장

학 번 : 2010-20272